Int. J. Electrochem. Sci., 16 **(2021)** Article ID: 210721, doi: 10.20964/2021.07.25

International Journal of
ELECTROCHEMICAL
SCIENCE
www.electrochemsci.org

Fabrication and Photoelectrochemical Performances of $BiFeO_3$ Thin Film Photoelectrodes: Effect of Annealing Temperature

Liqun Bai[1,], Xiaolin Li[1], Sen Wang[2], Hongjie Liu[3], Lu Shi[3], Qiuyue Luo[3], Wenlong Song[3], Da Chen[2,*]*

[1] Key Laboratory of Chemical Utilization of Forestry Biomass of Zhejiang Province, Zhejiang Agriculture and Forestry University, Hangzhou, Zhejiang Province, 311300, China
[2] College of Materials and Chemistry, China Jiliang University, Hangzhou, Zhejiang 310018, China
[3] Tianneng Battery Group Co., Ltd., Changxing City, Zhejiang 313100, China
[*]E-mail: bailiqun78@163.com, dchen_80@hotmail.com

Received: 6 March 2021 / *Accepted:* 16 April 2021 / *Published:* 31 May 2021

$BiFeO_3$ (BFO), as a ferroelectric material, has been considered as a new type of photoelectrode material in recent years and has been attracting extensive attention in many fields. In this work, pure phase BFO thin film photoelectrodes were successfully prepared by one-step sol-gel spin coating method, and the influence of annealing temperature on the structure and photoelectrochemical properties of BFO thin film photoelectrodes was also investigated. The XRD patterns and SEM images reveal that pure phase BFO with rhombohedral structure could be obtained under different annealing temperatures, and the BFO-550 thin film prepared at an annealing temperature of 550 ℃ had a more uniform and smooth thin film compared to those thin films prepared at an annealing temperature of 500 ℃, 600 ℃, or 650 ℃ (namely BFO-500, BFO-600, BFO-650). The transient photocurrent response spectra and linear sweep voltammetry (LSV) curves show that all the prepared BFO thin films exhibited good photoelectrochemical response characteristics, and the BFO-550 thin film photoelectrode possessed a much higher photoelectrochemical activity than the other BFO thin film photoelectrodes. The Mott-Schottky (M-S) curves, electrochemical impedance spectra (EIS) and photoluminescence (PL) spectra further indicate that the BFO-550 thin film photoelectrode had a higher carrier concentration, better photogenerated carrier separation efficiency and lower photo-generated carrier recombination rate than the other BFO thin film samples, thus leading to the improved photoelectrochemical activity of BFO-550. Moreover, the BFO-550 thin film photoelectrode could resist photocorrosion and exhibit relatively good photoelectrochemical stability, which should be beneficial to its photoelectrochemical applications.

Keywords: $BiFeO_3$ (BFO) thin film; Photoelectrode; Sol-gel; Annealing temperature; Photoelectrochemical performance

1. INTRODUCTION

Photoelectrochemistry is a technology that uses electrochemical processes under the action of light to convert or store solar energy into required chemical energy [1]. This technology has attracted extensive attention, and has been considered as one of the most effective ways to solve the two major problems of energy shortage and environmental pollution that human society is facing at present [2]. Generally, the key factor that affecting the photoelectrochemical performance lies in the thin film photoelectrode. Therefore, it is important for the development of photoelectrochemical technology to find a suitable low-cost and highly efficient thin film photoelectrode. As a ferroelectric material, $BiFeO_3$ (BFO) has many advantages [3-5], such as large spontaneous polarization (~100 $\mu C/cm^2$), small band gap (2.1~2.7 eV), good chemical stability and low cost. In virtue of these unique properties, BFO has been proven as a promising photoelectrode material for photoelectrochemical applications in recent years.

As known, the photoelectrochemical properties of semiconductor thin film photoelectrodes are mainly dependent on their crystal structure and surface properties, which are closely related to the preparation method and conditions [6, 7]. Due to its simple process, easy structure regulation and low cost, the sol-gel method has been developed as a common method for thin film preparation, and has also been widely used for the preparation of semiconductor thin film photoelectrodes (e.g., TiO_2 [8], Fe_2O_3 [9], ZnO [10, 11], $SrTiO_3$ [12]). For example, Singh et al. [13] successfully fabricated pure phase BFO and Mn-doped BFO thin film on $Pt/Ti/SiO_2/Si(100)$ substrate by a sol-gel method.

In this work, BFO thin film photoelectrodes were prepared by using an optimized sol-gel method, and the influence of annealing temperature on the crystal structure and photoelectrochemical performances of the prepared BFO thin films was further explored.

2. EXPERIMENTAL

2.1 Preparation of BFO thin film photoelectrodes

All chemicals were of analytical grade without further purification. The BFO thin film photoelectrodes were prepared by spin coating the BFO precursor sol on the surface of FTO conductive glass followed by being calcined at high temperature. The FTO conductive glass was firstly cleaned by ultrasonic washing with deionized water, isopropyl alcohol and ethanol for 15 min successively, and dried by nitrogen and then treated by ultraviolet ozone irradiation for 20 min before use. The BFO precursor sol was obtained as follows. 6 mmol of $Bi(NO_3)_3 \cdot 5H_2O$ was ultrasonically dissolved in 20 mL of ethylene glycol, followed by adding 10 mL of glacial acetic acid. Then, 6 mmol of $Fe(NO_3)_3 \cdot 9H_2O$ was added and also ultrasonically dissolved in the above solution. After that, 1 g of Pluronic P123 (PEO-PPO-PEO) as a surfactant was added to the above solution, which was continued with ultrasonic treatment for 30 min. After aging 24 h, the obtained precursor sol was then spin coated on the pretreated FTO surface at a speed of 1400 rpm for 40 s under ambient conditions. The prepared precursor thin films were thermally treated on a hotplate at 150°C for 30 min, and were then annealed in a muffle furnace at

different high temperatures (i.e., 500, 550, 600, or 650°C) for 20 minutes. After cooling naturally to room temperature, the BFO thin film photoelectrode was thus obtained. The BFO thin film photoelectrode samples obtained at different annealing temperatures were named BFO-500, BFO-550, BFO-600 and BFO-650, respectively.

2.2 Characterizations

The crystalline structures of the obtained different BFO thin films were determined by a Bruker D2 Advance X-ray diffractometer using Cu K_α radiation ($\lambda = 0.15406$ nm). The morphological features of the prepared BFO thin films were examined by using field emission scanning electron microscopy (FESEM, Hitachi SU8010). The photoluminescence (PL) spectra were performed on a Hitachi High-Tech F-7000 fluorescence spectrophotometer at an excitation of 407 nm.

2.3 Photoelectrochemical measurements

The photoelectrochemical performances of the prepared BFO thin film photoelectrodes were evaluated on a CHI660E electrochemical workstation with a home-built three-electrode photoelectrochemical cell in 0.5 M Na_2SO_4 aqueous solution, in which a platinum wire was used as a counter electrode, a saturated Ag/AgCl electrode was used as reference electrode and the fabricated BFO thin film photoelectrode was used as working electrode. A 300 W xenon arc lamp assembled with an optical filter ($\lambda \geq 420$ nm) was used as a visible light source, and the average irradiance intensity was calibrated to be 100 mW cm^{-2}. The linear sweep voltammetry (LSV) curves were measured at a scanning rate of 10 mV s^{-1}, and the transient photocurrent response measurements were performed upon intermittent visible light ($\lambda \geq 420$ nm) irradiation at 0 V (vs. Ag/AgCl) potential bias. The Mott-Schottky (M-S) curves were acquired at an applied frequency of 1 kHz in the voltage range from -0.8 V to + 0.2 V in the dark. The electrochemical impedance spectra (EIS) were recorded with a frequency range from 10 mHz to 100 kHz using an AC amplitude perturbation of 5 mV under visible light irradiation ($\lambda \geq 420$ nm).

3. RESULTS AND DISCUSSION

3.1 Structural and morphological features

Figure 1 shows the X-ray diffraction (XRD) patterns of all the BFO thin film samples prepared at different annealing temperatures. As seen, all the BFO thin film samples had similar XRD patterns, except for the different diffraction peak intensities. The characteristic diffraction peaks appearing at 22.4, 31.8, 32.1, 39.5 and 56.9 degrees corresponded to the (012), (104), (110), (202) and (214) crystal planes of the rhombohedral BFO (JCPDS No.36-1415), respectively, and the rest of characteristic peaks belonged to the FTO conductive substrate. This indicates that the crystalline BFO thin films were successfully fabricated on the FTO surface through a sol-gel method. Meanwhile, the diffraction peak

intensity of the prepared BFO thin films increased with the increase of annealing temperature. That is to say, the increased annealing temperature could improve the crystallinity of BFO thin films, manifesting that the annealing temperature had a great influence on the crystallization performance of BFO thin films.

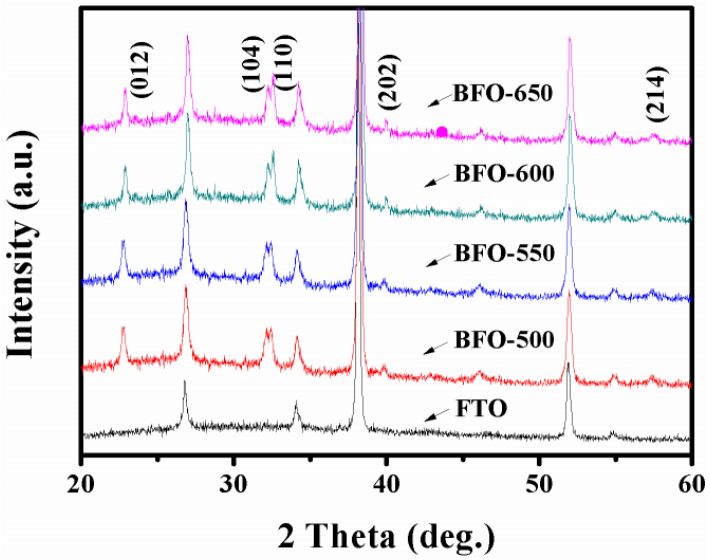

Figure 1. XRD patterns of the prepared BFO thin films at different annealing temperatures

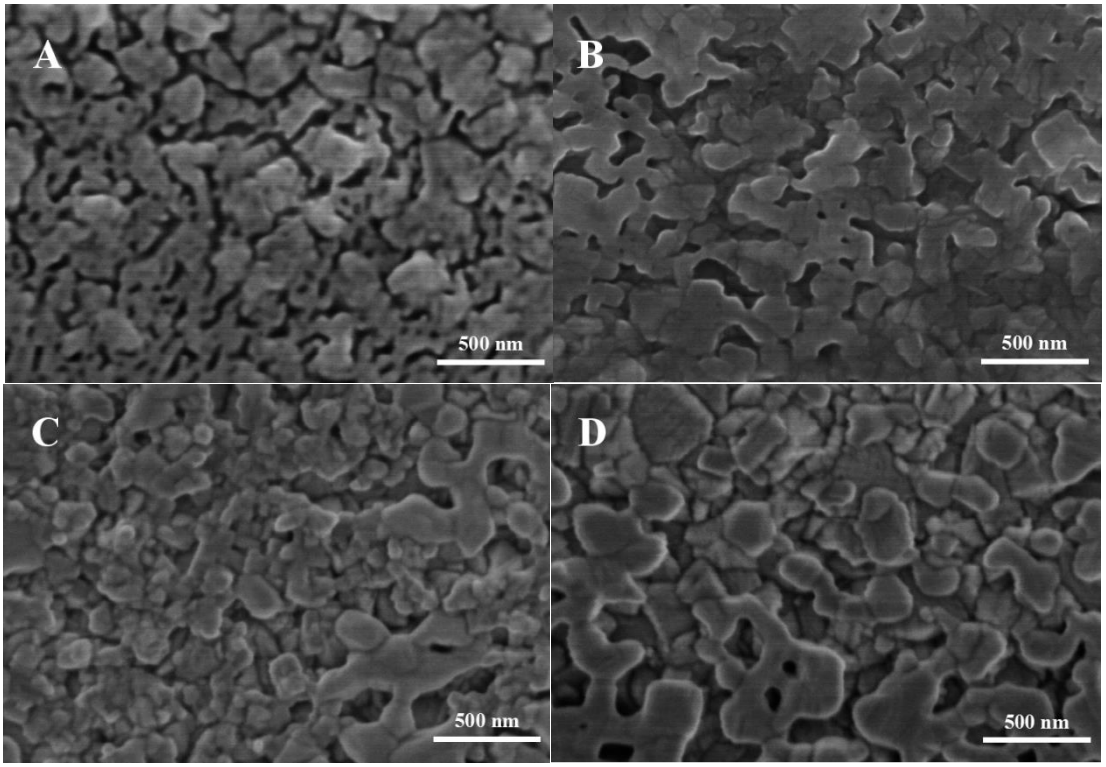

Figure 2. FESEM image of the prepared BFO thin film samples: (A) BFO-500; (B) BFO-550; (C) BFO-600, (D) BFO-650.

The morphological features of the prepared BFO thin films were investigated by FESEM. As shown in Figure 2, all the prepared BFO thin films were composed of irregular nanoparticles with a particle size of about 50~300 nm, and most of these nanoparticles were connected to each other. For the BFO-500 thin film sample, there were obvious voids between the particles on the thin film surface, thus making the film density relatively poor. This was largely due to the insufficient annealing temperature that affected the film-forming property of the sol. However, with the increase of annealing temperature, the surface density of the prepared BFO thin film was greatly improved. Moreover, compared with the BFO-600 and BFO-650 thin film samples, the BFO-550 thin film sample possessed a relatively more uniform and smooth surface morphology, which would probably facilitate the separation and migration of photogenerated carriers within the thin film and ultimately improve the corresponding photoelectrochemical performance.

3.2 Photoelectrochemical performance

In order to evaluate the influence of annealing temperature on the photoelectrochemical performance of the BFO thin film, the transient photocurrent response spectra of the prepared BFO thin film photoelectrode were examined.

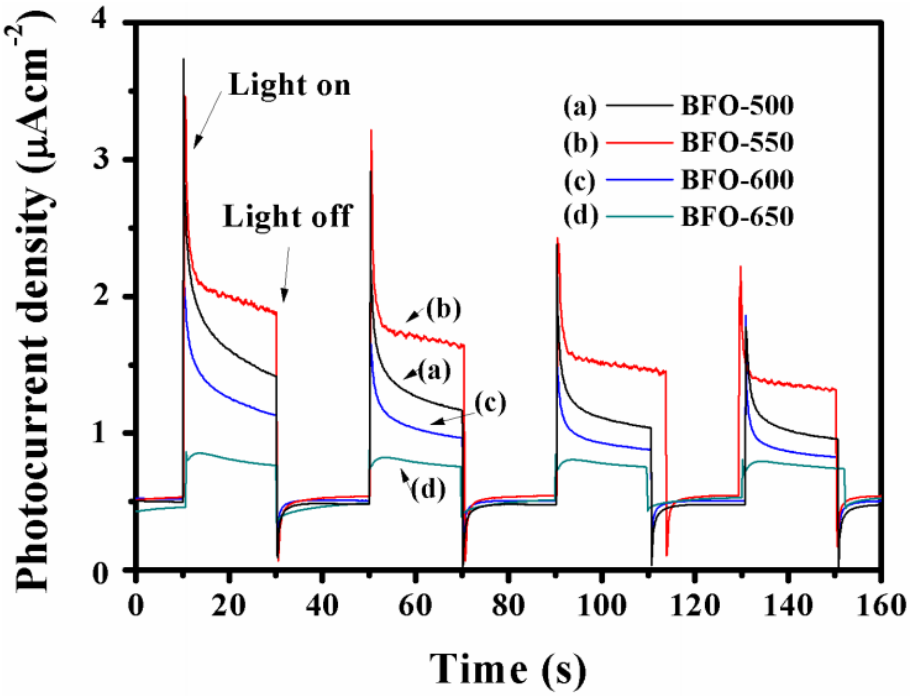

Figure 3. Transient photocurrent responses of the prepared BFO thin film samples measured in 0.5 M Na_2SO_4 solution at 0 V (vs. Ag/AgCl) under the irradiation of 300 W xenon lamp.

Figure 3 presents the transient photocurrent response spectra of the prepared BFO thin film samples. It can be seen that the photocurrent intensity of the BFO thin film firstly increased when the annealing temperature rised from 500 ℃ to 550 ℃, and then decreased when the annealing temperature further increased to 600 ℃ and 650 ℃. This may be attributed to the following fact: (1) the initial

increase of annealing temperature could improve the crystallinity of BFO films and reduce the internal defects of the thin films, thus leading to the increase of photocurrent intensity; (2) when the annealing temperature further increased, the surface roughness of the thin film would also increase, making the migration distance of photogenerated carriers within the thin film surface increase accordingly, which may lead to the increase of internal recombination rate and thus the decrease of photocurrent intensity [14]. Moreover, the transient photocurrent response measurements can also reflect the interfacial electron hole recombination rate of the photoelectrode. As seen in Figure 3, when the light was on or off, the instantaneous abnormal peak photocurrent could be clearly observed. When the light was on, the flux of photogenerated hole instantly into the surface of the BFO thin film resulted in the generation of the transient peak photocurrent, which would then rapidly attenuate to the steady state due to the recombination of the photogenerated holes and photogenerated electrons. When the light was off, the cathode photocurrent also appeared in a similar situation, because the photogenerated-electron flux migrated instantaneously to the photoelectrode surface and then recombined with the existing photogenerated holes on the surface [15]. This phenomenon indicates that the surface of BFO thin film had a relatively high recombination rate of photogenerated electrons and holes. Therefore, how to reduce the recombination of photogenerated electrons and holes will be a key issue to be considered in our future research.

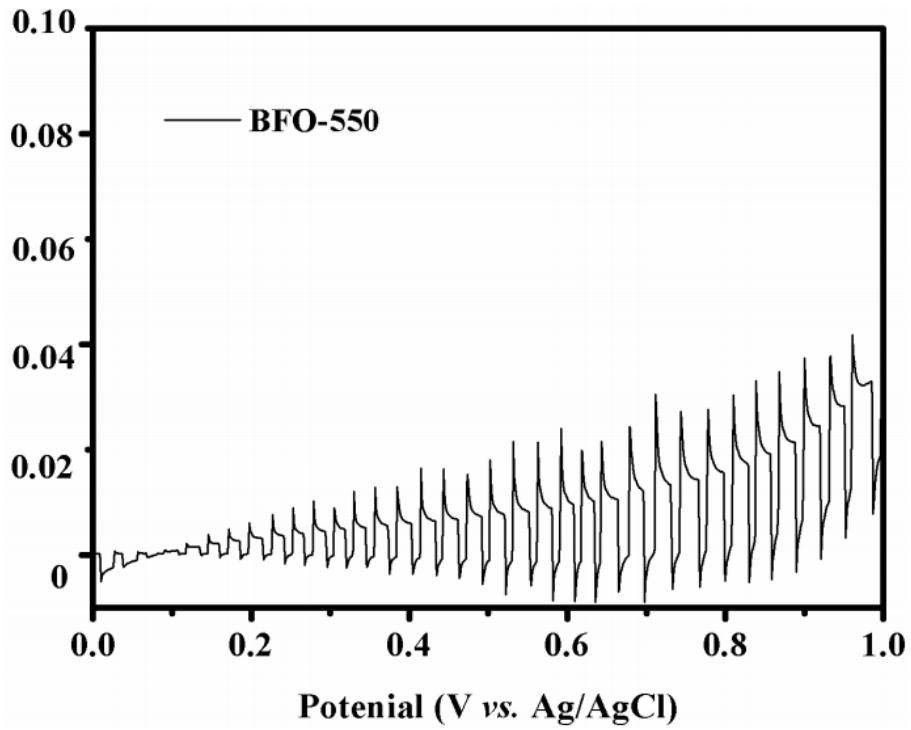

Figure 4. Chopped light LSV of the prepared BFO-550 thin film photoelectrode measured in 0.5 M Na_2SO_4 solution under the irradiation of 300 W xenon lamp.

The LSV curve is of great importance in the analysis of the photoelectrochemical response. Figure 4 shows the LSV curve of the prepared BFO-550 thin film photoelectrode upon chopped light irradiation with a scan rate of 10 mV/s. It can be seen that the photocurrent density increased gradually

with the increase of voltage during the process of linear scanning. Meanwhile, in each voltage scanning interval, it can be observed that the photocurrent density immediately increased to the abnormal peak value and then rapidly decayed to the steady state when the light was on, while the photocurrent density also immediately decreased to the abnormal negative peak value and then quickly returned to the steady state when the light was off. The LSV results further confirm that the prepared BFO thin film photoelectrode had a good photocurrent response performance.

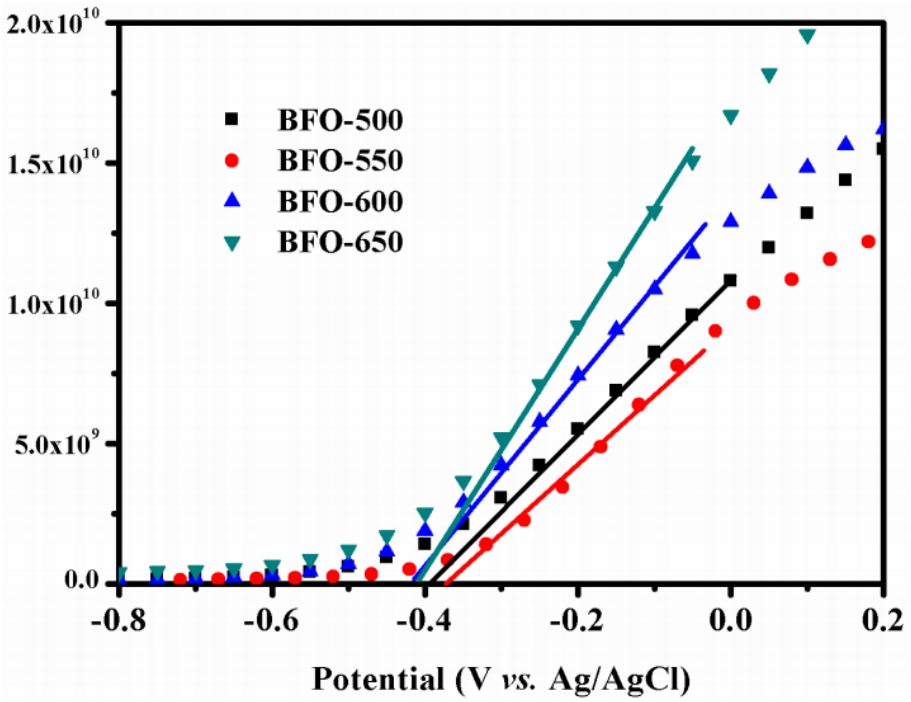

Figure 5. Mott-Schottky curves of the prepared BFO thin film photoelectrodes measured in 0.5 M Na_2SO_4.

To further investigate the effect of annealing temperature on the photoelectrochemical properties of BFO thin films, we estimated the charge carrier concentration on different sample surfaces by Mott-Schottky (M-S) spectra. Figure 5 shows the M-S spectra of the different BFO thin film photoelectrode samples prepared at different annealing temperatures. As seen, the slopes of M-S curves of all the thin film photoelectrodes were positive, indicating that all the prepared BFO thin films were n-type semiconductor materials, which is consistent with the previously reported literature [16, 17]. Moreover, according to Mott-Schottky's formula [18, 19], the slope of M-S curve is inversely proportional to carrier concentration (N_D). It can be seen that the order of carrier concentration of BFO thin film samples obtained at four different annealing temperatures was as follows: BFO-550 > BFO-500 > BFO-600 > BFO-650, which is consistent with the order of the magnitude of the transient photocurrent response as shown in Figure 3. This result confirms that a higher carrier concentration in the semiconductor generally means a greater charge transfer capacity of the semiconductor, which is probably more conducive to the photoelectrochemical reaction process.

In order to investigate the interfacial photogenerated charge separation efficiency of thin film photoelectrode, the electrochemical impedance measurements were performed on the BFO thin film photoelectrodes prepared at different annealing temperatures, and the EIS results are shown in Figure 6. As shown, the EIS curves of different BFO thin film photoelectrodes exhibited significantly different arc radii, of which BFO-550 had the smallest arc radius, followed by BFO-500, BFO-600 and BFO-650. In general, a smaller arc radius in the EIS curve means a more efficient separation of photogenerated electrons and holes [20].

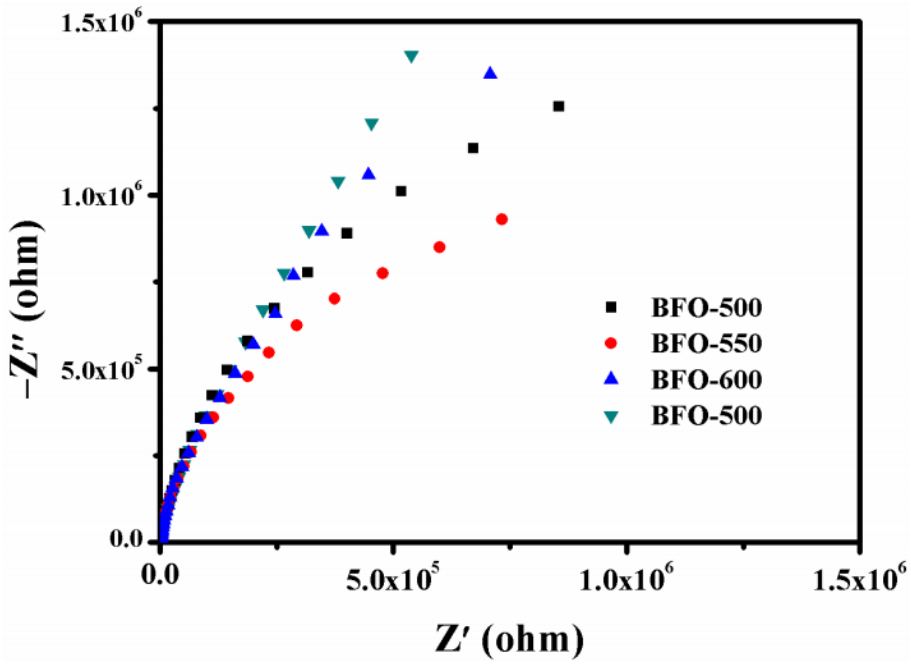

Figure 6. EIS curves of the prepared BFO thin film photoelectrodes measured in 0.5 M Na_2SO_4.

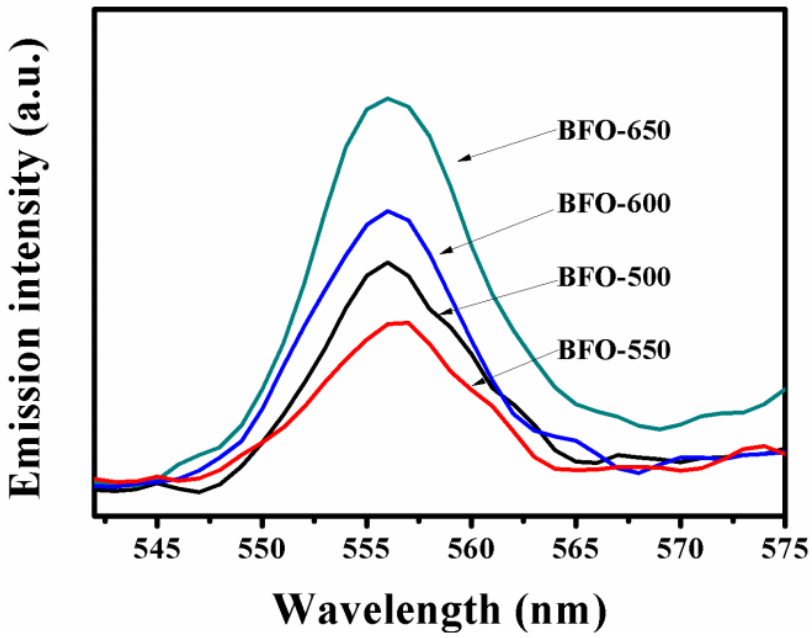

Figure 7. PL spectra of the prepared BFO thin film photoelectrodes.

Therefore, compared with BFO-500, BFO-600 and BFO-650, the BFO-550 thin film photoelectrode had a more efficient separation efficiency of photogenerated carriers, thus promoting the photoelectrochemical process to a large extent. This further explains why the transient photocurrent density of BFO-550 was better. In addition, the recombination ability of photogenerated electrons and holes can be reflected from the photoluminescence (PL) spectra, and it is generally believed that a lower PL intensity means a lower recombination ability of photogenerated carriers [21]. Figure 7 shows the PL spectra of BFO thin film photoelectrodes prepared at different annealing temperatures. It can be observed that the order of the PL intensity was as follows: BFO-550 < BFO-500 < BFO-600 < BFO-650. Apparently, the BFO-550 thin film photoelectrode had the lowest PL intensity, indicating that the BFO-550 thin film photoelectrode exhibited the lowest photogenerated carrier recombination ability, thus greatly improving the photoelectrochemical performance.

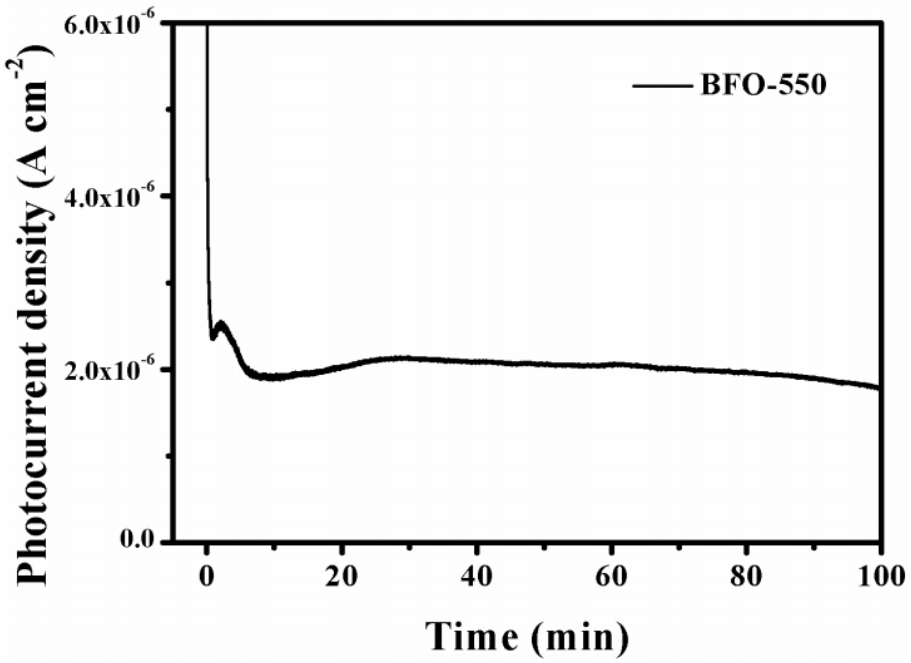

Figure 8. Photoelectrochemical stability measurement of the prepared BFO-550 thin film photoelectrode at 0 V (vs. Ag/AgCl).

As known, the photoelectrochemical stability of thin film photoelectrodes is crucial for their practical photoelectrochemcial applications. With this in mind, the photoelectrochemical stability of the prepared BFO thin film photoelectrode was also investigated. Figure 8 shows the photocurrent density of the prepared BFO-550 thin film photoelectrode changing with the illumination time upon continuous irradiation for 100 minutes. As can be seen, the photocurrent density of BFO-550 did not change significantly during the whole illumination time, indicating that the prepared BFO thin film photoelectrode possessed a relatively strong photocorrosion resistance and a good photoelectrochemical stability. Such excellent stability will inevitably benefit the potential practical applications of BFO thin film photoelectrodes in the photoelectrochemical field.

4. CONCLUSION

In this work, the sol-gel spin coating method combined with a high temperature annealing process was employed to prepare BFO thin film photoelectrodes, and the influence of annealing temperature on the structural morphology and photoelectrochemical performance of the prepared BFO thin film photoelectrode was also explored. It was found that all the BFO thin film photoelectrodes prepared at different annealing temperatures were rhombohedral phase structure, and these thin films were composed of irregular nanoparticles with a particle size of 50~300 nm connected together. In particular, the BFO-550 thin films prepared at 550 ℃ were more uniform and smooth than other thin films prepared at 500 ℃, 600 ℃ and 650 ℃. The transient photocurrent response results show that the BFO-550 thin film photoelectrode exhibited much higher photocurrent density and better photoelectrochemical properties than the other three BFO thin film photoelectrodes (i.e., BFO-500, BFO-600 and BFO-650). According to the results of Mott-Schottky, EIS and PL spectra, the BFO-550 thin film photoelectrode possessed a more carrier concentration, a more efficient photogenerated carrier mobility and a lower photogenerated carrier recombination efficiency, which should be the main reasons for the better photoelectrochemical performance of BFO-550. In addition, the prepared BFO thin film photoelectrode also displayed good photoelectrochemical stability, which is beneficial to the practical photoelectrochemical applications of BFO thin film photoelectrode.

ACKNOWLEDGEMENTS
This work was financially supported by the Zhejiang Provincial Natural Science Foundation of China (No. LY19E020003, LQ20F040007, LQ19F040004), National Natural Science Foundation of China (No. 51972294).

References

1. L. Wang, M. Schmid and J. B. Sambur, *J. Chem. Phys.*, 151 (2019) 180901.
2. C. R. Jiang, S. J. A. Moniz, A. Q. Wang, T. Zhang and J. W. Tang, *Chem. Soc. Rev.*, 46 (2017) 4645.
3. T. Zhao, A. Scholl, F. Zavaliche, K. Lee, M. Barry, A. Doran, M. P. Cruz, Y. H. Chu, C. Ederer, N. A. Spaldin, R. R. Das, D. M. Kim, S. H. Baek, C. B. Eom and R. Ramesh, *Nat. Mater.*, 5 (2006) 823.
4. F. Gao, X. Y. Chen, K. B. Yin, S. Dong, Z. F. Ren, F. Yuan, T. Yu, Z. G. Zou and J. M. Liu, *Adv. Mater.*, 19 (2007) 2889.
5. P. F. Yuan, H. Y. Zhou, Z. M. Wang, J. Q. Deng, P. Liu and Q. R. Yao, *Int. J. Electrochem. Sci*., 12 (2017) 3686.
6. Y. M. He, T. Hamann and D. W. Wang, *Chem. Soc. Rev*., 48 (2019) 2182.
7. E. Archela, L. P. de Camargo, M. R. D. Pelissari and L. H. Dall'Antonia, *Int. J. Electrochem. Sci.*, 14 (2019) 3581.
8. S. Kityakarn, Y. Pooarporn, P. Songsiriritthigul, A. Worayingyong, S. Robl, A. M. Braun and M. Wörner, *Electrochim. Acta*, 83 (2012) 113.
9. Y. Li, N. Guijarro, X. L. Zhang, M. S. Prévot, X. A. Jeanbourquin, K. Sivula, H. Chen and Y. D. Li, *ACS Appl. Mater. Interfaces*, 7 (2015) 16999.
10. L. Znaidi, *Mater. Sci. Eng*. B, 174 (2010) 18.
11. A. R. Nimbalkar, N. B. Patil, V. V. Ganbavle, S. V. Mohite, K. V. Madhale and M. G. Patil, *J. Alloys Compd.*, 775 (2019) 466.
12. D. H. Bao, X. Yao, N. Wakiya, K. Shinozaki and N. Mizutani, *Appl. Phys. Lett*., 79 (2001) 3767.

13. S. K. Singh, H. Ishiwara and K. Maruyama, *Appl. Phys. Lett*., 88 (2006) 262908.
14. P. S. Shewale, S. H. Lee and Y. S. Yu, *J. Alloy Compd*., 744 (2018) 849.
15. C. Y. Cummings, F. Marken, L. M. Peter, A. A. Tahir and K. G. Upul Wijayantha, *Chem. Commun*., 48 (2012) 2027.
16. S. J. A. Moniz, R. Quesada-Cabrera, C. S. Blackman, J. W. Tang, P. Southern, P. M. Weaver and C. J. Carmalt, *J. Mater. Chem*. A, 2 (2014) 2922.
17. Y. Z. Wang, D. Chen, S. Wang, J. H. Liang, L. S. Qin, X. G. Sun and Y. X. Huang, *J. Electrochem. Soc*., 166 (2019) D308.
18. K. P. S. Parmar, H. J. Kang, A. Bist, P. Dua, J. S. Jang and J. S. Lee, *ChemSusChem*, 5 (2012) 1926.
19. S. Wang, D. Chen, F. Niu, N. Zhang, L. S. Qin and Y. X. Huang, *RSC Adv.,* 6 (2016) 34574.
20. Y. Lv, Y. Zhu and Y. Zhu, *J. Phys. Chem*. C, 117 (2013) 18520.
21. Y. Yao, G. Li, S. Ciston, R. M. Lueptow and K. A. Gray, *Environ. Sci. Technol*., 42 (2008) 4952.